Electronic Supplementary Material (ESI) for Journal of Materials Chemistry C.


# Tuning the Phase Stability and Surface HER Activity of 1T′-$MoS_2$ by Covalent Chemical Functionalization

Jiu Chen, Fuhua Li, Yurong Tang* and Qing Tang*

School of Chemistry and Chemical Engineering, Chongqing Key Laboratory of Theoretical and Computational Chemistry, Chongqing University, Chongqing 401331, China

*To whom correspondence should be addressed. E-mail: tangyuronga@cqu.edu.cn; qingtang@cqu.edu.cn.

## Abstract

The metallic phase of 1T′-$MoS_2$ has triggered versatile investigations owing to its high activity towards hydrogen evolution reaction (HER) both on the edges and basal plane. However, the structural instability of the metastable 1T′-$MoS_2$ restricts its practical applications. Covalent functionalization has been widely used to modify the intrinsic properties of low-dimensional nanomaterials. Here, we explore the potential of covalent chemical functionalization in modulating the stability and catalytic activity of the 1T′-$MoS_2$ monolayer by first-principles calculations. We probed the benchmark H and a series of carbon-terminated functional groups, and found that surface functionalization via formation of covalent S-H or S-C bonds can effectively stabilize 1T′-$MoS_2$ against its conversion back to the 2H phase. The critical coverage needed for 1T′ stabilization is 33.3% for H and 25.0% for the C-terminated groups. Different from the semi-metallic character of pristine 1T′-$MoS_2$, the electronic structure of chemically functionalized

1T′-$MoS_2$ is adsorbate-dependent, which can be a semiconductor or metal. Moreover, compared to the pristine 1T′-$MoS_2$, we identified the -$CH_2CH_2OH$ and -$CH_2COOH$ functionalized 1T′-$MoS_2$ can well balance the electrocatalytic HER activity and stability, and the activity at some of the surface S sites even outperforms the pristine 1T′-$MoS_2$. This study provides useful chemical route to control the phase stability, electronic properties and electrocatalytic performances of thermodynamically unstable 1T′-$MoS_2$ and other transition metal dichalcogenides.

## Introduction

Hydrogen has the potential to be a carbon free and clean energy source. It can be potentially realized by splitting water with light[1] or electricity[2], which are the most promising solutions to the scalable and sustainable production of $H_2$ without carbon emissions. Although platinum and other noble metals present the most efficient catalytic performance for the hydrogen evolution reaction (HER),[3] their commercial applications are largely hindered by their scarcity and high cost.

Recently, molybdenum disulfide ($MoS_2$), one of the most popular catalytic two-dimensional (2D) materials other than graphene, has been urging abundant exploration as promising alternative to platinum and noble materials for HER.[4-7] The bulk of $MoS_2$, however, has an indirect band gap[8] and poor HER activity.[9] As for the $MoS_2$ monolayer, a direct band gap was observed when $MoS_2$ was exfoliated into monolayer.[10] Monolayer $MoS_2$ has two typical structure phase: the 2H phase with trigonal prismatic Mo-coordination and the 1T phase with octahedral Mo-coordination.[11, 12] The 2H phase is semiconducting and thermodynamically stable, while the 1T phase is metallic and unstable, which can easily convert into the meta-stable 1T′ phase with distorted octahedral coordination. The 2H form has been widely studied for hydrogen evolution. In 2005, Nørskov et al.[5] theoretically predicted that the electrocatalytic active sites lie on the edges of 2H $MoS_2$ nanoparticles and the basal plane is catalytically inactive, which was later confirmed by experiment in 2007.[6] Since then, extensive research attentions have been dedicated to increasing the number of active sites of 2H edges or

defects.[13-17] However, the catalytic activity of the semiconducting 2H $MoS_2$ is still limited by its intrinsic properties.[18, 19]

On the other hand, nanosheets of $MoS_2$ made by chemical exfoliation can partially convert the 2H phase into the metallic 1T′ phase.[20-22] More interestingly, transformation of the semiconducting 2H-$MoS_2$ to the metallic 1T′-$MoS_2$ can remarkably enhance the HER catalytic activity.[23-26] Unlike the 2H phase where the catalytic sites only locate at the edges, the basal plane as well as the edges of 1T′-$MoS_2$ are both catalytically active for HER.[23] Hence, the phase control of $MoS_2$ monolayer is more important for enhancing the HER activity. Note that although 1T′-$MoS_2$ is active for HER, the instability of 1T′ remains a great concern, impeding its electrocatalytic applications. This has, thus, triggered enormous efforts to stabilize the 1T′ phase. For example, previous studies showed that doping rhenium can retain the stability of 1T′-$MoS_2$.[27] Lately, chemical functionalization has been applied in experiment [28-30] as a new route to stabilize the metastable 1T′- $MoS_2$ and tune the electrocatalytic properties.[29, 31] Nonetheless, the recent experiments revealed that the functional groups with organic phenyl rings can increase the 1T′ stability at the cost of decreasing the HER reactivity compared to the pristine 1T′ phase.[26, 32]

Despite the recent experimental exploration on the phase-engineering and reactivity of functionalized 1T′-$MoS_2$, the impact of covalent functionalization by versatile functional groups on the stability, electronic properties and the basal-plane HER reactivity of the 1T′-$MoS_2$ is elusive. Several other related works[31-34] have also reported on the stability and electrocatalytic activity of 1T′-$MoS_2$ by covalent

functionalization, yet those previous theoretical studies mainly focus on the simple H groups. An atomic-level understanding and comparison on the stability and surface activity tuned by different types of functional groups has been lacking. In practice, we expect to seek for a surface modifier that can effectively stabilize the 1T′-$MoS_2$, inhibiting its conversion back to the semiconducting 2H state, and at the same time, can keep or even outperform the catalytic HER activity of the pristine 1T′-$MoS_2$.

In this study, we performed systematic density functional theory (DFT) studies of functionalized $MoS_2$ attached by a series of different functional groups (-H, -$NO_2$Ph, -$CH_2COOH$, -$CH_2CONH_2$, -$CH_2CH_2OH$, -$NH_2$Ph, -$CH_3$, herein all of the selected modifiers have been used in experiment for functionalization) to investigate the effect of surface modifiers on the stability, electronic structures, and HER activity of 1T′-$MoS_2$. It is found that the 1T' structure will be greatly stabilized against the 2H phase when the functional group coverage reaches up to 25%. We also investigated the electronic structures of the functionalized 1T′-$MoS_2$. An evident band gap is opened for H functionalization, while the C-functional groups result in semiconducting or metallic properties. Finally, the stabilized 1T′-$MoS_2$ structures were used to study the electrocatalytic activity. Using the pristine 1T′-$MoS_2$ as the benchmark, we found that most of the studied functional groups tend to decrease the surface HER activity, while -$CH_2CH_2OH$ and -$CH_2COOH$ are identified to be able to significantly boost the HER reactivity with close-to-zero H* adsorption free energy.

**Computational methods**

We built the periodic 2×3×1 rectangular supercells of 2D 1T′-$MoS_2$ and 2H-$MoS_2$ monolayers as the model systems. The vacuum layer is more than 15 Å to avoid interlayer interaction. The first Brillouin zone was sampled by Gamma-centered 3×3×1 k-point mesh. The first-principle computations of all the structures were performed on the Vienna ab initio simulation package (VASP 5.4.4)[35] by using projector augmented wave (PAW)[36] method to describe the ion-electron interaction. The functional of Perdew, Burke, Ernzerhof (PBE) of generalized gradient approximation (GGA)[37] was adopted to represent the electron exchange-correlation. The cutoff energy of plan-wave basis set was set to be 400 eV. A DFT-D3 dispersion correction was carried out to describe the van der Waals (vdW) interactions between the functional groups and the substrate. The convergence criterion for structural optimization were $10^{-5}$ eV for energy and -0.02 eV/Å for residual force. During structural optimizations, the dipole corrections are included along the z-axis direction (Table S1). All the structures were fully relaxed and the pristine 1T and 2H phase are dynamically stable with no imaginary frequency from phonon spectra (Figure S1a and 1b). For the functionalized systems, due to the large computational cost for phonon calculations, we examined their stabilities by performing the AIMD[38-40] calculations at 300K for 5 ps. We take the functionalized 1T and 2H phase with H at 33.3% coverage and $–CH_3$ at 25% coverage as the representatives to study the dynamic stability (Figure S1c to 1f ), which show no structural reconstruction after the MD simulations, indicating the stability of the functionalized $MoS_2$.

The Gibbs free energy change of hydrogen adsorption ($\Delta G_H$) on the surface of functionalized 1T′-$MoS_2$ was defined by

$$\Delta G_H = \Delta E_H + \Delta E_{ZPE} - T\Delta S_H,$$

where $\Delta E_H$, $\Delta E_{ZPE}$ and $\Delta S_H$ are the change of the total energy, differences of the zero-point energy and change of the entropy at the 298.15K, respectively. $\Delta E_H$ is defined as the following equation:

$$\Delta E_H = E_H - 1/2\ E_{H_2} - E_{cat}$$

in which $E_H$, $E_{cat}$, $E_{H_2}$ indicate the electronic energy of the functionalized 1T′-$MoS_2$ with and without hydrogen, and the free hydrogen molecule, respectively.

**Results and discussion**

**Functionalization by H benchmark functional groups.**

Previous literatures have showed that H can functionalize the 1T′-$MoS_2$ and tune the electronic properties.[31, 34] Here we use H as the testing group to explore the favorable double-side adsorption sites of both the 2H and 1T′ phase. The hydrogen is covalently attached to the sulfur atom layer of $MoS_2$ at various coverage, spanning from 8.3% to 50%. Note that we did not consider higher coverage since only 50% surface sulfur atoms in 1T′-$MoS_2$ that are close to the Mo atomic layer (denoted as $S_t$ site in Figure 1a) are catalytically more active for HER.[20] Another consideration is that higher H coverage (> 50%) in the 2H-$MoS_2$ is structurally unstable, and the adsorbed H tends to desorb from the surface in the form of $H_2$ molecule. In order to obtain the most stable configuration at each hydrogen concentration, we examine all the possible surface adsorption sites (Figure S2). There are two distinct sulfur sites in 1T′ phase (the tensile

S site ($S_t$) and the compressive S site ($S_c$), Figure 1a), and only one type of sulfur site in 2H phase. At the same time, we also take into account the different bonding modes of H to the surface S, and both the upright and the slant hydrogen adsorption are considered. We found that all the examined hydrogens favor the upright H adsorption over the 1T′ phase, while the slant H adsorption is preferred over the 2H phase.

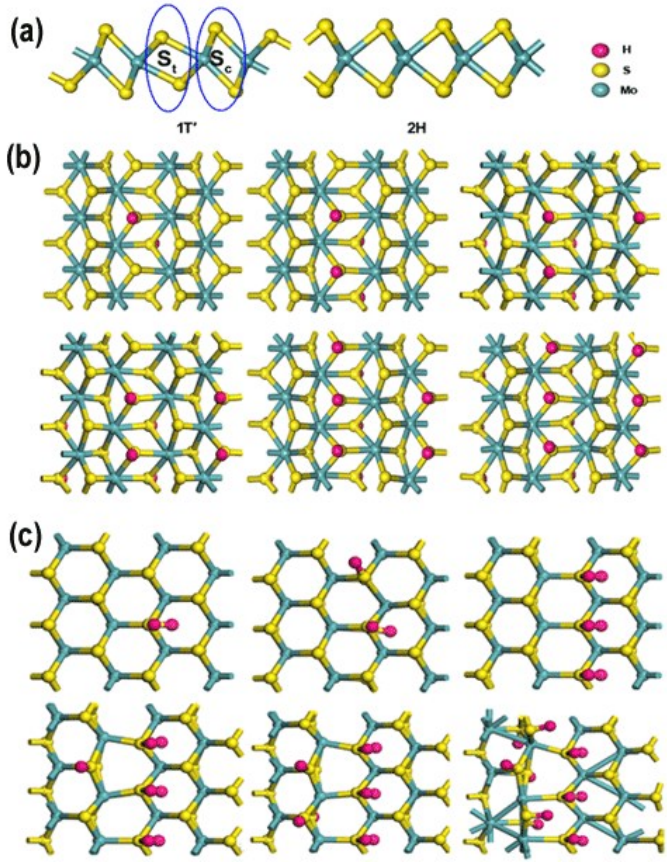


**Figure 1.** The structure models of free-standing 1T′-$MoS_2$ and 2H-$MoS_2$ (a), the distinctive surface S sites on 1T′-$MoS_2$ are shown. The most stable configurations of H-functionalized 1T′-$MoS_2$ (b) and 2H-$MoS_2$ (c) as a function of different H coverage via double-site adsorption. Color modes: pink for H, yellow for S, and green for Mo.

The most stable structures of the double-side H adsorption over the hydrogenated 2H- and 1T′-$MoS_2$ at different coverage are shown in Figure 1b and 1c, and the optimized lattice parameters as well as the total energies are provided in Table S2 and

S3. It is apparent that the $S_t$ site of 1T′-$MoS_2$ is the major site for hydrogen adsorption. By comparison, the $S_c$ site is relatively inert for hydrogen adsorption. This is consistent with the higher surface reactivity of the sulfur atoms at the $S_t$ site. Another interesting observation is that the absorbed hydrogen atoms are isolated at lower coverage and form hydrogen lines along the $S_t$ site at higher coverage until all the $S_t$ sites are occupied at the coverage of 50%. In the case of 2H-$MoS_2$ phase, we found that the adsorbed hydrogens are inclined to be clustered rather than being dispersedly distributed. Note that the distribution of surface hydrogen is quite similar to the distribution of the chalcogen vacancies in the 1T′ and 2H phase.[41] Moreover, from the Figure 1, one can see that the functionalization of 1T′ phase still remains the structure and symmetry of the metallic phase with the increasing H coverage, suggesting the potential of stability and catalytic activity of the modified 1T′-$MoS_2$ monolayer. However, the 2H phase has a severe distortion in the Mo-S structural framework.

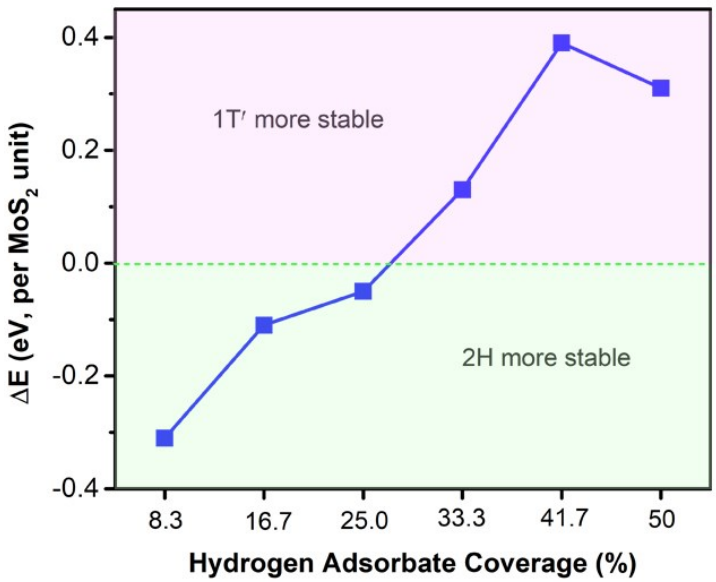


**Figure 2.** The energy difference (ΔE) between the H-modified 2H- and 1T′-$MoS_2$ as a function of H coverage. The energy difference is defined as $\Delta E = (E_{2H} - E_{1T'})$/number of $MoS_2$ unit, $E_{2H}$ and

$E_{1T'}$ represents the electronic energy of H functionalized 2H- and 1T′-$MoS_2$ at the same coverage. The negative ΔE indicates the 2H phase is more stable, while the positive ΔE indicates the 1T′ phase is more stable.

In particular, we also investigated the relationship between phase stability and surface functionalization by comparing the energetics of the 1T′ and 2H phase at various hydrogen coverage (Figure 2). Initially, the functionalized 1T′ phase is less stable than the 2H phase at the onset coverage of 8.3%. Then, as the adsorbed H increases, the energy difference between them decreases. Particularly, the 1T′ phase is stabilized by the H groups and becomes more stable against the 2H phase when the H coverage increases to 33.3%. Hence, surface functionalization can lead to improved and better thermodynamic stability in the 1T′ phase and prevent the phase transformation to the semiconducting 2H phase.

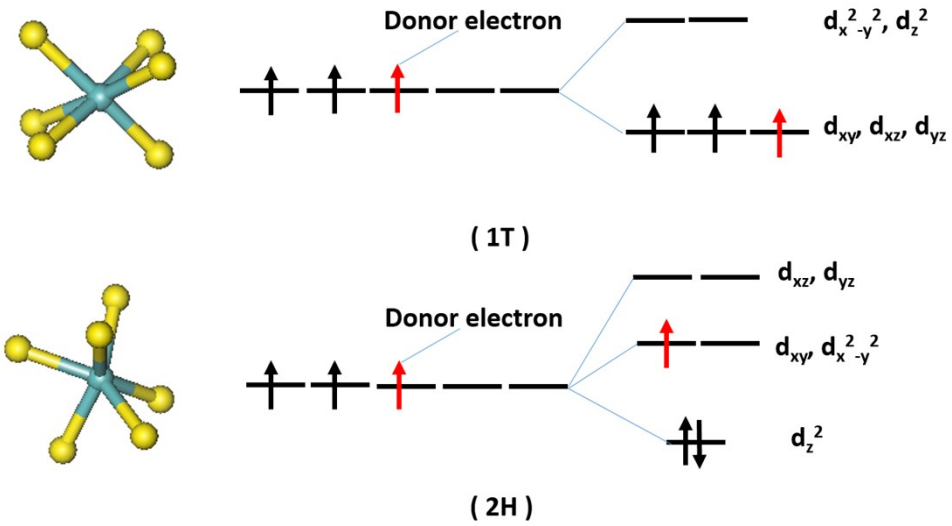


**Figure 3.** The states of Mo 4d orbital in 1T- and 2H-$MoS_2$ after accepting one donor electron, as indicated by the red arrow.

Then the question is: how to understand this interesting stabilizing mechanism? Gotthard Seifert et al. [27] has previously proposed a stabilizing mechanism based on the

crystal field theorem. They showed that the top of the valence band and the bottom of the conduction band are composed by the Mo 4d states in 2H-$MoS_2$, and the metallic Mo 4d states host the Fermi level in 1T′-$MoS_2$.[27] In terms of the crystal field theory, the Mo 4d states are split into three groups in 2H-$MoS_2$ and two groups in 1T-$MoS_2$ (Figure 3). The incomplete occupation of Mo $4d_{xy,yz,xz}$ orbitals leads to the metallic ground state of 1T-$MoS_2$, but it also decreases the stability. Noteworthy, here we chose the perfect 1T structure to explain the difference in the orbital occupancy with the 2H phase since it is the important precursor of distorted 1T' phase when phase transition occurs from 2H to 1T′ via surface S layer sliding. For the distorted octahedral coordination, due to the Jahn-Teller effect, the triply degenerate $t_{2g}$ ($d_{xy,yz,xz}$) will further split into two groups of d-orbitals with small energy level differences. When the H as electron donor attaches to the $MoS_2$ monolayer, the additional electron of 1T-$MoS_2$ occupies the partially occupied Mo $4d_{xy,yz,xz}$ orbitals and enhances the stability due to the half-full occupation of the Mo $4d_{xy,yz,xz}$ orbitals. Bader charge analysis indeed showed that there is about 0.085 |e| transferred from each adsorbed H to 1T′-$MoS_2$. By contrast, the excess electron of 2H-$MoS_2$ fills the vacant $4d_{xz}$ or $4d_{x^2-y^2}$ orbital, leading to the metallic-like electronic structure and destabilizing the lattice of the 2H-$MoS_2$ nanosheets. Consequently, the H atom can serve as a functional group to stabilize the 1T′-$MoS_2$ and destabilize the 2H-$MoS_2$.

**Functionalization by carbon-terminated organic groups.**

Our above discussion have indicated that hydrogen adatom functionalization can effectively stabilize the 1T′ phase against 2H by binding with the surface sulfur atom

layer. Driven by the boosting stability of 1T′-$MoS_2$, how the stability of 1T′ and 2H phase is influenced by other types of functional groups and at what coverage will the 1T′ structure becomes stabilized would need further investigations. Herein, we use -$CH_3$ as the test example to examine the optimal adsorption sites. The surface St site in 1T′ phase is preferred for C-terminated groups adsorption (Table S4), and the binding sites at different coverage are shown in Figure S3, e.g. – $CH_3$. The pattern models of –$CH_3$ on 1T′-$MoS_2$ are quite similar to the H, except for the 16.7% coverage. However, the pattern models on the 2H-$MoS_2$ are different from the H case, possibly due to the steric hindrance from the neighboring surface sites. Based on the favorable adsorption sites, the –$CH_3$ groups are replaced by other carbon-terminated functional groups, including -$NO_2$Ph,[32] -$CH_2$COOH,[29] -$CH_2CONH_2$,[28] -$CH_2CH_2$OH,[42] -$NH_2$Ph, [32] and attached to the surface sulfur atom layer of 1T′ and 2H phase by S-C bond at different coverage (from 8.3% to 33.3%). Here we should emphasize that we did not consider the higher coverage above 33.3% due to the bulky steric effect and repulsion interaction of the large organic groups. In this series, the optimized lattice parameters are listed in Table S2, which generally exhibit an increasing trend in lattice with the increasing number of the added functional groups. This suggests that the increase of functional groups can enlarge the $MoS_2$ lattice and may cause tensile strain to the Mo-S framework.

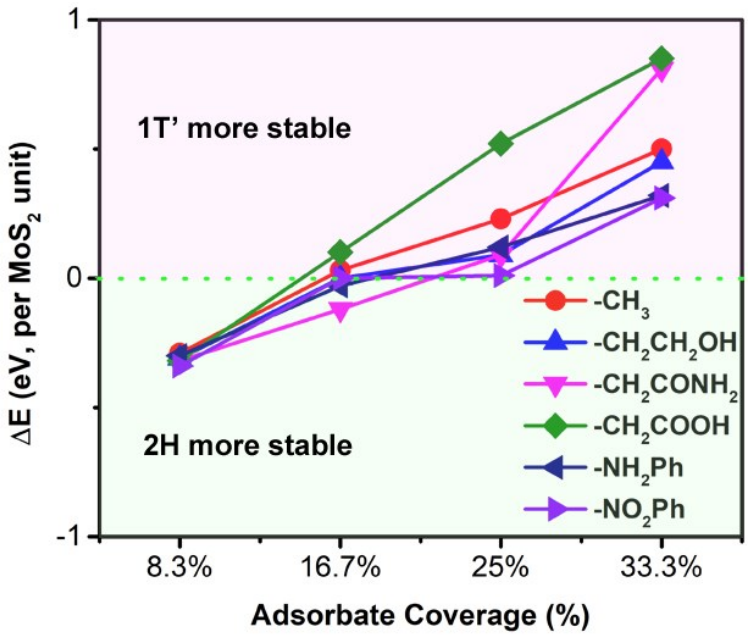


**Figure 4.** The curve of ΔE (eV, per $MoS_2$ unit) as a function of the carbon-containing functional group coverage. $\Delta E(eV)=(E_{2H}-E_{1T'})$/number of $MoS_2$ unit, $E_{2H}$ and $E_{1T'}$ represents the electronic energy of functionalized 2H and 1T′ with coverage from 8.3% to 33.3%. The 1T′ phase is more stable when the ΔE is positive (above zero, indicated by the purple area).

Here, differences in total energy from DFT calculations (ΔE) between the modified 1T′- and 2H-$MoS_2$ (the data of total energy differences are listed in Table S5) are used to evaluate the phase stability. It is clear that ΔE (Figure 4) grows monotonously from negative to positive, and changes the sign after 16.7% before 25.0%, whatever the types of the withdrawing or donating electron groups. Thus, similar to the hydrogen functionalization, the adsorption of carbon-terminated functional groups can also decrease the energy difference between 2H and 1T′ phase, resulting in more stabilized 1T′ phase with the coverage reaching up to 25%. We should note that the carbon-containing groups require less functional group coverage (lower or

close to 25%) on the $MoS_2$ monolayer than the H group (33.3%) to make the 1T′ phase energetically more favorable.

To explore the reason why different functional groups lead to the same effect on the stability of 1T′-$MoS_2$, we performed the Bader charge calculations. The Bader charge analysis (Table 1) shows that there is substantial amount of charge (0.03 ~ 0.12 |e|) transferred from each functional group to $MoS_2$ monolayer, which means the 1T′-$MoS_2$ can gain extra electrons from the surface modifiers. We also checked the charge transfer with HSE06 functional and the results shows that there is a small difference of about 0.02 |e| on the supercell (~0.003 |e| for each functional group), which has no effect on our results quantitatively. Interestingly, we observe a larger charge transfer from the electron donating groups (e.g., -$NH_2$Ph, -$CH_3$, -$CH_2CH_2OH$) to $MoS_2$ than that from the electron withdrawing groups (e.g., -$NO_2$Ph, -$CH_2COOH$, -$CH_2CONH_2$). More interestingly, the electron withdrawing or donating groups are both losing electron (Table 1). Thus, the 1T′-$MoS_2$ substrate functions as an electron acceptor, and the gained additional electron occupies the incompletely occupied Mo $4d_{xy,yz,xz}$ orbitals, stabilizing the 1T′ phase. These results can explain the similar impact of the electron withdrawing and donating groups on the stability of 1T′-$MoS_2$.

**Table 1.** The charge on each functional group (-R) of the functionalized 1T′-$MoS_2$ at the H coverage of 33.3% and C-terminated group coverage of 25%.

| -R | -$NO_2$Ph | -$NH_2$Ph | -$CH_3$ | -$CH_2CH_2OH$ | H | -$CH_2COOH$ | -$CH_2CONH_2$ |
|---|---|---|---|---|---|---|---|
| charge($e^-$) | 0.067 | 0.085 | 0.100 | 0.118 | 0.085 | 0.029 | 0.080 |

**Electronic structures.**

The band structure can give us an additional insight into the changes of electronic properties. The calculated band structures at the PBE-GGA level of the pristine and modified 1T′-$MoS_2$ by different functional groups are shown in Figure 5. The bare 1T′-$MoS_2$ monolayer is semimetallic with close-to-zero band gap (0.04 eV, Figure 5a). The opening of a tiny band gap is in good agreement with previous predictions by others (0.04 eV,[43, 44] 0.03 eV[45] and 0.08 eV[46]). After functionalization, the 1T′ phase demonstrates varying electronic properties. The H functionalized 1T′-$MoS_2$ at 33.3% coverage has a direct and larger band gap of 0.53 eV (Note that the H coverage can affect the band gap of 1T′-$MoS_2$, which has a 0.03 eV indirect gap for 8.3 % coverage, and metallic for 16.7% and 25% coverage.), while the C-functionalized 1T′-$MoS_2$ at lower 25% coverage exhibit metallic character for $-CH_2CH_2OH$, $-CH_2COOH$, and -$NO_2Ph$. Differently, the 1T′-$MoS_2$ functionalized by -$NH_2Ph$ and $-CH_2CONH_2$ exhibits small indirect band gap of 0.17 eV and 0.01 eV, respectively. Another interesting observation is that the band becomes more flat with lower dispersion compared to the pristine 1T′-$MoS_2$. This is possibly owing to the localized surface S-C bonds after functionalization. Thus, in addition to the structural stability, the electronic properties of 1T′-$MoS_2$ can also be effectively and flexibly modulated through varying different kinds of functional groups.

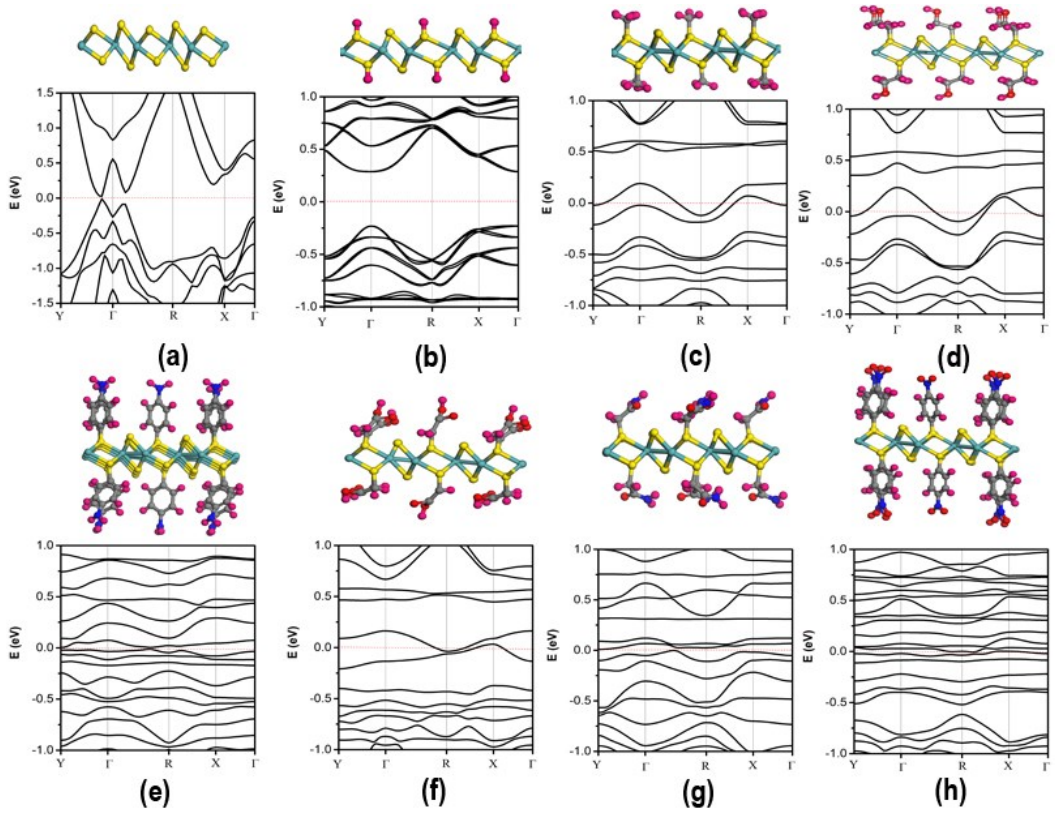


**Figure 5.** The band structures of pristine and functionalized 1T -$MoS_2$ by different functional groups (the coverage is 33.3% for H and 25% for the C-terminated groups) (a) pristine, (b) -H, (c) -$CH_3$, (d) -$CH_2CH_2OH$ (e) -$NH_2Ph$ (f) -$CH_2COOH$, (g) -$CH_2CONH_2$, (h) -$NO_2Ph$.

**HER activity of functionalized 1T′-$MoS_2$.**

Noteworthy, the presence of functional groups would block the reactive S sites. However, the surface sulfur atoms of the chemically stabilized 1T′-$MoS_2$ are not fully passivated, leaving the unfunctionalized surface S as the potential active sites for hydrogen evolution. Thus, we further studied the catalytic activity of the stabilized 1T′-$MoS_2$ configuration for HER (33.3% coverage for H and 25% coverage for the C-terminated groups). Here we only investigated the hydrogen adsorption on single-side of the functionalized 1T′ phase. All the possible hydrogen adsorption sites (Figure 6a,

Table S6) over the un-functionalized $S_t$-type sulfur were examined, including site 1, 2, and 3 (here for H functionalization at 33.3%, site 3 is occupied by H, and site 1 and 2 are geometrically equivalent). The change of Gibbs free energy ($\Delta G_H$) is used to evaluate the HER activity. An efficient HER electrocatalyst should have a moderate H affinity (neither too weak nor too strong, and the ideal value is thermo-neutral).

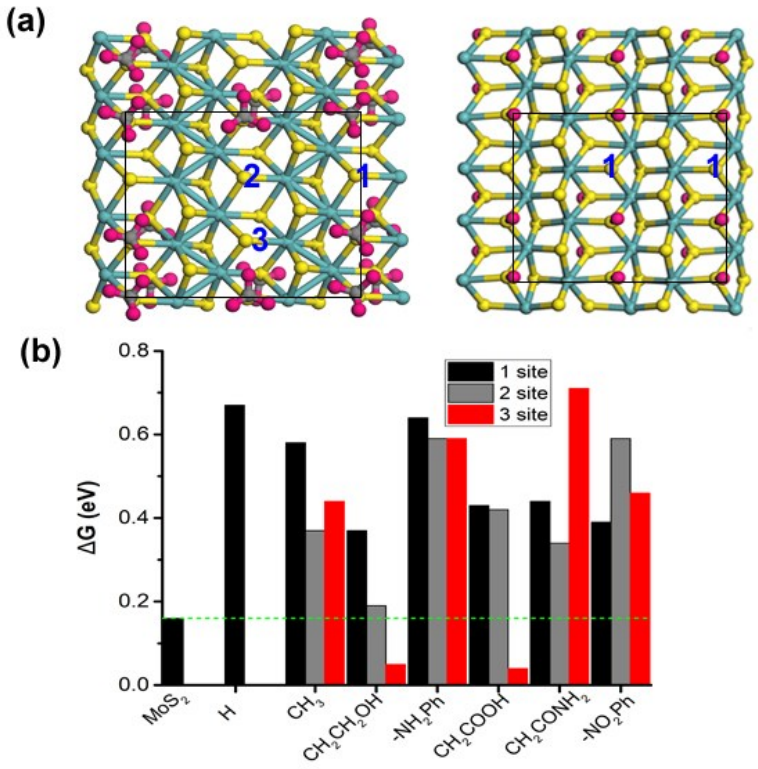


**Figure 6.** (a) The three possible H adsorption sites of C-group functionalized 1T′-$MoS_2$ at coverage of 25% (left). For H-functionalized 1T′-$MoS_2$ at coverage of 33.3%, site 3 is pre-occupied by H, and site 1 and site 2 are equivalent (right). The rectangular area indicates the supercell used for calculations. (b) The change in Gibbs free energy of H adsorption over the different adsorption sites.

In Figure 6b, the calculations show that the values of $\Delta G_H$ exhibit strong dependence on the adsorption sites, and that on the surface 3 site of 1T′-$MoS_2$ functionalized by $-CH_2CH_2OH$ and $-CH_2COOH$ are 0.05 and 0.03 eV, respectively,

more close to 0 than that of the pristine 1T′-$MoS_2$ (0.16 eV, the green benchmark line). This reflects that this type of 1T′ phase functionalization is more active than the bare metastable 1T′-$MoS_2$ for HER on site 3. Besides, the HER activity of site 2 on the basal plane of $^{-}CH_2CH_2OH$-functionalized 1T′ phase is slightly lower ($\Delta G_H$ = 0.20 eV), but is also highly active for HER. By comparison, the surface S atoms of 1T′ phase covalently modified by the other functional groups tend to decrease the HER reactivity, as indicated by the much higher $\Delta G_H$ between 0.3 to 0.7 eV, regardless of the adsorption sites. These findings suggest that although chemical functionalization provides an effective way to enhance the structural stability of 1T′-$MoS_2$, the surface HER activity has to be sacrificed for most of the investigated functional groups. To establish the correlation between the electronic structure and the HER activity, Table S7 summarizes the band gap, the HP value (Hammett parameter that indicates the electron-donating or -withdrawing ability), and the calculated $\Delta G_H$ for all of the investigated functional groups. However, we found no direct correlation between the band gap or HP value and the $\Delta G_H$. A possible reason is that except for the electronic structure, the local structural strain might also contribute to the HER activity, since different functional groups with different steric effect can lead to the varying lattice parameter and local surface strain. We should note that the recent experimental finding by Benson et al. also showed that the 1T′ phase functionalized with the organic phenyl rings such as -$NO_2$Ph and -$NH_2$Ph exhibits slightly worse HER activity compared to the pristine metallic 1T′-$MoS_2$, which is qualitatively consistent with our theoretical predictions.[32] Additional experimental studies are highly expected to verify our other predictions and establish the relation

between the type of functional groups on 1T′-$MoS_2$ and the corresponding HER performance.

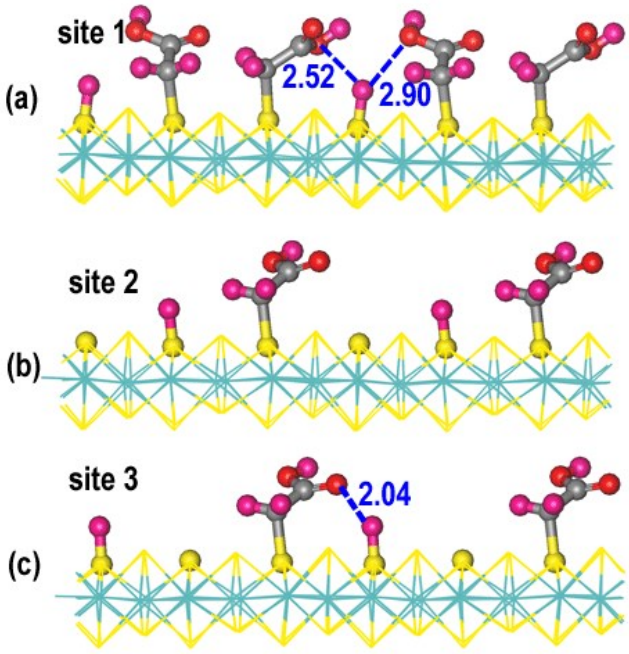


**Figure 7.** Geometry of H adsorption at different surface sites on –$CH_2COOH$ modified 1T′-$MoS_2$.

Furthermore, a more detailed analysis showed that, at each available un-attached surface S (site 1, 2, 3), the H binding is relatively stronger over the −$CH_2CH_2OH$-modified 1T′-$MoS_2$ ($\Delta G_H$ is lower and closer to the 1T′-$MoS_2$ benchmark). Hence, among the studied functional groups, the moderate electron-donating −$CH_2CH_2OH$ would be the better choice to balance the structural stability and the long-term HER performance. Noteworthy, the 1T′-$MoS_2$ is stabilized against the 2H phase by obtaining extra charge from the functional groups, and the electron-donating groups can have larger amount of charge transfer to stabilize the 1T′ phase. Interestingly, the electron-withdrawing −$CH_2COOH$ also leads to optimal HER activity at the site 3, while the activity at site 1 and 2 is relatively poor. In order to understand this difference, we analyzed the bonding geometries of H adsorption. At site 3, there is a unique interaction

of hydrogen bond between the adsorbed hydrogen and the carbonyl oxygen from the −$CH_2COOH$ group (H···O distance of 2.04 Å) (Figure 7c). The formation of hydrogen bonding is only observed at site 3, which is, however, geometrically absent at site 1 or site 2. This interaction plays an extremely important role in stabilizing the energetics of the adsorbed hydrogen.

**Perspectives**.

Our study in this work has demonstrated that covalent surface functionalization by the organic functional groups are able to effectively protect the 1T′-$MoS_2$ monolayer and flexibly tune the electronic properties and surface HER activity. In most cases, the structural stability can be greatly enhanced, while the electrocatalytic activity has to compromise. Fortunately, we identified $-CH_2CH_2OH$ and $-CH_2COOH$ are the potential candidates to balance the catalytic activity and structural stability. Besides the functional groups examined in this study, the impact of more versatile functional groups beyond hydrogen or carbon binding to sulfur, like, oxygen, nitrogen, fluorine, chlorine and so forth, is worth further explorations. In addition, this functionalization method can be extended to other 2D TMDs nanosheets to modify their intrinsic properties and expand the TMDs family applications.

## Conclusions

In summary, we have theoretically explored the stability, electronic structures and HER activity of covalently functionalized $MoS_2$ by the benchmark H and carbon-terminated functional groups. We found that surface functionalization via formation of covalent S-H or S-C bonds can effectively protect and stabilize the meta-stable 1T′-

$MoS_2$. The critical coverage needed for 1T′ stabilization against transformation to the 2H phase is predicted to be 33.3% for H and 25% for the C-terminated groups. Furthermore, we showed that functionalization leads to significant changes in electronic structures, and the 1T′-$MoS_2$ monolayer can be semiconducting or metallic depending on the adsorbate varied. Despite the enhanced structural stability, the catalytic HER activity is compromised for most of the examined functional groups. Only -$CH_2CH_2OH$ and -$CH_2COOH$ functionalized 1T′ phases are identified to exhibit promising activity, and the HER activity at some of the surface sites even surpasses that of the pristine 1T′-$MoS_2$, which can balance between the electrocatalytic activity and stability. We believe that these understandings can help us find the effective route to stabilize the catalytically reactive but thermodynamically metastable 1T′ phase and retain or even boost the surface HER activity by the covalent chemistry.

**Notes**

The authors declare no competing financial interests.

**Supporting Information**

The phonon dispersion and AIMD results, the possible hydrogen and –$CH_3$ adsorption sites, the optimal lattice parameters, the energy difference of functionalized 2H and 1T′ phase, the change of free energy of H adsorption at sites 1, 2, and 3.

**Acknowledgements**

This work was supported by the National Natural Science Foundation of China (No.21903008), the Chongqing Municipal Resources and Society Security Bureau (cx2019141), the Chongqing Science and Technology Commission (cstc2020jcyj-

msxmX0382), and the Fundamental Research Funds for the Central Universities (2020CDJQY-A031, 2020CDJ-LHZZ-063). This research used resources of the National Supercomputer Center in Guangzhou.

**References**

1 M. S. Dresselhaus, I. L.Thomas, *Nature* **2001**, *414*, 332-337.

2 J. A. Turner, *Science* **2004**, *305*, 972-974.

3 S. Trasatti, *J. Electroanal. Chem.* **1972**, *39*, 163-184.

4 M. A. Lukowski, A. S. Daniel, F. Meng, A. Forticaux, L. S. Li, S. Jin, *J. Am. Chem. Soc.* **2013**, *135*, 10274-10277.

5 B. Hinnemann, P. G. Moses, J. Bonde, K. P. Jorgensen, J. H. Nielsen, S. Horch, I. Chorkendorff, J. K. Norskov, *J. Am. Chem. Soc.* **2005**, *127*, 5308-5309.

6 K. P. J. Thomas F. Jaramillo, Jacob Bonde, Jane H. Nielsen, I. C. Sebastian Horch, *Science* **2007**, *317*, 100-102.

7 J. Kibsgaard, Z. Chen, B. N. Reinecke, T. F. Jaramillo, *Nat. Mater.* **2012**, *11*, 963-969.

8 K. K. Kam, B. A. Parkinson, *J. Phys. Chem.* **1982**, *86*, 463-467.

9 W. Jaegermann, H. Tributsch, *Progr. Surf. Sci.* **1988**, *29*, 1-167.

10 K. F. Mak, C. Lee, J. Hone, J. Shan, T. F. Heinz, *Phys. Rev. Lett.* **2010**, *105*, 136805.

11 C. Ataca, H. Sahin, S. Ciraci, *J. Phys. Chem. C* **2012**, *116*, 8983-8999.

12 J. Heising, M. G. Kanatzidis, *J. Am. Chem. Soc.* **1999**, *121*, 638-643.

13 D. Kong, H. Wang, J. J. Cha, M. Pasta, K. J. Koski, J. Yao, Y. Cui, *Nano Lett.* **2013**, *13*, 1341-1347.

14 Y. Li, H. Wang, L. Xie, Y. Liang, G. Hong, H. Dai, *J. Am. Chem. Soc.* **2011**, *133*, 7296-7299.

15 J. Xie, H. Zhang, S. Li, R. Wang, X. Sun, M. Zhou, J. Zhou, X. W. Lou, Y. Xie, *Adv. Mater.* **2013**, *25*, 5807-5813.

16 J. Benson, M. Li, S. Wang, P. Wang, P. Papakonstantinou, *ACS Appl. Mater. Inter.* **2015**, *7*, 14113-14122.

17 H. I. Karunadasa, E. Montalvo, Y. J. Sun, M. Majda, J. R. Long, C. J. Chang, *Science* **2012**, *335*, 698-702.

18 A. B. Laursen, S. Kegnæs, S. Dahl, I. Chorkendorff, *Energy Environ. Sci.* **2012**, *5*, 5577-5591.

19 D. Merki, S. Fierro, H. Vrubel, X. Hu, *Chem. Sci.* **2011**, *2*, 1262-1267.

20 X. L. Fan, Y. Yang, P. Xiao, W. M. Lau, *J. Mater. Chem. A* **2014**, *2*, 20545-20551.

21 G. Eda, T. Fujita, H. Yamaguchi, D. Voiry, M. W. Chen, M. Chhowalla, *ACS Nano* **2012**, *6*, 7311-7317.

22 G. Eda, H. Yamaguchi, D. Voiry, T. Fujita, M. W. Chen, M. Chhowalla, *Nano Lett.* **2012**, *12*, 526-526.

23 D. Voiry, M. Salehi, R. Silva, T. Fujita, M. Chen, T. Asefa, V. B. Shenoy, G. Eda, M. Chhowalla, *Nano Lett.* **2013**, *13*, 6222-6227.

24 U. Maitra, U. Gupta, M. De, R. Datta, A. Govindaraj, C. N. Rao, *Angew. Chem. Int. Ed. Engl.* **2013**, *52*, 13057-13061.

25 Q. Liu, X. Li, Q. He, A. Khalil, D. Liu, T. Xiang, X. Wu, L. Song, *Small* **2015**, *11*, 5556-5564.

26 C. Tsai, K. R. Chan, J. K. Norskov, F. Abild-Pedersen, *Surf. Sci.* **2015**, *640*, 133-140.

27 A. N. Enyashin, L. Yadgarov, L. Houben, I. Popov, M. Weidenbach, R. Tenne, M. Bar-Sadan, G. Seifert, *J. Phys. Chem. C* **2011**, *115*, 24586-24591.

28 D. Voiry, A. Goswami, R. Kappera, C. e Silva Cde, D. Kaplan, T. Fujita, M. Chen, T. Asefa, M. Chhowalla, *Nat. Chem.* **2015**, *7*, 45-49.

29 J. I. Paredes, J. M. Munuera, S. Villar-Rodil, L. Guardia, M. Ayan-Varela, A. Pagan, S. D. Aznar-Cervantes, J. L. Cenis, A. Martinez-Alonso, J. M. D. Tascon, *ACS Appl. Mater. Inter.* **2016**, *8*, 27974-27986.

30 K. C. Knirsch, N. C. Berner, H. C. Nerl, C. S. Cucinotta, Z. Gholamvand, N. McEvoy, Z. X. Wang, I. Abramovic, P. Vecera, M. Halik, S. Sanvito, G. S. Duesberg,

V. Nicolosi, F. Hauke, A. Hirsch, J. N. Colernan, C. Backes, *ACS Nano* **2015**, *9*, 6018-6030.

31 Q. Tang, D. E. Jiang, *Chem. Mater.* **2015**, *27*, 3743-3748.

32 E. E. Benson, H. Zhang, S. A. Schuman, S. U. Nanayakkara, N. D. Bronstein, S. Ferrere, J. L. Blackburn, E. M. Miller, *J. Am. Chem. Soc.* **2018**, *140*, 441-450.

33 Q. Tang, D.-e. Jiang, *ACS Catal.* **2016**, *6*, 4953-4961.

34 Y. Y. Linghu, N. Li, Y. P. Du, C. Wu, *Phy. Chem. Chem. Phys.* **2019**, *21*, 9391-9398.

35 G. Kresse, J. Furthmuller, *Phys. Rev. B* **1996**, *54*, 11169-11186.

36 P. E. Blochl, *Phys. Rev. B* **1994**, *50*, 17953-17979.

37 J. P. Perdew, K. Burke, M. Ernzerhof, *Phys. Rev. Lett.* **1996**, *77*, 3865-3868.

38 B. Akgenc, *Comput. Mater. Sci.* **2020**, *171*, 109231.

39 B. Akgenc, A. Mogulkoc, E. Durgun, *J. Appl. Phys.* **2020**, *127*, 084302.

40 A. Bafekry, B. Akgenc, M. Ghergherehchi, F. M. Peeters, *J. Phys. Condens. Matter.* **2020**, *32*, 355504.

41 Q. Tang, *J. Mater. Chem. C* **2018**, *6*, 9561-9568.

42 L. Ries, E. Petit, T. Michel, C. C. Diogo, C. Gervais, C. Salameh, M. Bechelany, S. Balme, P. Miele, N. Onofrio, D. Voiry, *Nat. Mater.* **2019**, *18*, 1112-1118.

43 B. Ouyang, S. Chen, Y. Jing, T. Wei, S. Xiong, D. Donadio, *J. Materiomics* **2018**, *4*, 329-337.

44 D. Saha, S. Mahapatra, *Phys. Chem. Chem. Phys.* **2017**, *19*, 10453-10461.

45 S. J. R. Tan, S. Sarkar, X. Zhao, X. Luo, Y. Z. Luo, S. M. Poh, I. Abdelwahab, W. Zhou, T. Venkatesan, W. Chen, S. Y. Quek, K. P. Loh, *ACS Nano* **2018**, *12*, 5051-5058.

46 X. Qian, J. Liu, L. Fu, J. Li, *Science* **2014**, *346*, 1344-1347.